Mon. Not. R. astr. Soc. (1984) **211,** 679–693

The remarkable kinematics of the WR wind-blown bubble RCW 58

L. J. Smith★ and M. Pettini *Royal Greenwich Observatory, Herstmonceux Castle, Hailsham, East Sussex BN27 1RP*

J. E. Dyson *Department of Astronomy, The University, Manchester M13 9PL*

T. W. Hartquist *Astronomy Program, University of Maryland, College Park, MD 20742, USA*

Accepted 1984 June 28. Received 1984 May 30; in original form 1984 March 15

Summary. We present high resolution, high signal-to-noise ratio, ultraviolet and optical observations of HD 96548, a WN8 star surrounded by the nebula RCW 58 which consists of stellar ejecta enclosed in a wind-blown bubble. The spectra exhibit blueshifted absorption components in a number of interstellar lines arising from a variety of ions. The velocities of the components are well correlated with their ionization potentials in the sense that C IV has the highest velocity relative to the star ($v_{LSR}=-150\,km\,s^{-1}$) and Fe II the lowest ($v_{LSR}=-102\,km\,s^{-1}$). We discuss the likely origin of such a correlation, of which this is the first example discovered, and argue that the absorption components arise behind the inwards-facing shock within the wind-blown bubble. Significant modifications to the standard bubble model are, however, required by our results; in particular the slope of the velocity/ionization potential relationship is too high for a simple post-shock flow. We propose that a non-simple flow occurs in which the hot shocked stellar wind material mixes with cold stellar ejecta and cools as it flows outwards and decelerates. This mixing process can, at least for RCW 58, explain the lack of energy conservation in WR shells.

1 Introduction

Some Wolf–Rayet (WR) stars are associated with nebulae having the shape of a ring or an arc centred on and photoionized by the WR star. These so-called 'ring nebulae' form a distinct class of H II regions and indicate some form of interaction between the central WR stars and their interstellar environments. WR stars associated with ring nebulae have been reported by several

★Present address: Department of Physics and Astronomy, University College London, Gower Street, London WC1E 6BT.

authors (e.g. Johnson & Hogg 1965; Crampton 1971). More recently Chu (1981) and Heckathorn, Bruhweiler & Gull (1982) have completed systematic sky surveys and compiled catalogues which show that overall 19 galactic WR stars are associated with ring nebulae. Several mechanisms have been suggested for the formation of ring nebulae. Johnson & Hogg (1965) proposed that the shells are composed of interstellar material which has been swept up by the central WR stellar winds. Wendker *et al.* (1975) alternatively suggested that the shells are composed of material shed by the central star in the process of becoming a WR star. Chu (1981) has performed a detailed kinematic and morphological study of 15 WR ring nebulae and finds that both these mechanisms occur, although the former is more usual.

The interaction of a stellar wind with the ambient interstellar medium has been studied by various authors (e.g. Pikel'ner 1968; Avedisova 1972; Dyson & de Vries (1972); Falle (1975); and Weaver *et al.* 1977). The evolutionary picture that emerges may be divided into three phases. During the first several thousand years the stellar wind produces an adiabatically expanding spherical bubble. Subsequently, radiative losses in the swept-up gas dominate leading to the formation of a thin shell. Finally the expansion slows to the ambient sound speed and the shell is dissipated. Pikel'ner (1968) showed that during the thin shell phase four distinct regions exist: (1) the stellar wind bounded by an inwards-facing shock; (2) shocked stellar wind with $T>10^6$ K; (3) a shell of shocked interstellar gas bounded by an outwards-facing shock; and (4) the ambient interstellar medium. In this model, the shell of shocked interstellar material is driven by the expansion of the hot bubble of gas which is energy conserving because the gas is too hot to cool efficiently.

The validity of this model has, however, recently been put into question by two observational results apparently in contradiction with theoretical predictions. In their study of five WR ring nebulae, Treffers & Chu (1982) and Chu (1982) found that the ratio of the observed kinetic energy of the WR shells to the total energy output of the WR stellar winds is about a factor of 10 less than the theoretically predicted value of 0.2 for an energy-conserving bubble. Another disagreement with theory was shown by the results of Kwitter (1981) for the WR ring nebula NGC 6888. She found that the WR stellar wind is thoroughly mixed into the swept-up shell, whereas the contact discontinuity between the bubble and shell only allows mixing to occur through evaporation of the shell into the bubble.

To address these and other related questions we have begun a study of ring nebulae in absorption against the central WR stars. As part of this programme, we have obtained ultraviolet and optical spectra of the WN8 star HD 96548 which is surrounded by the nebula RCW 58. Chu (1982) has studied the morphology of RCW 58 and concluded that it consists of stellar ejecta immersed in a wind-blown bubble. The stellar ejecta are characterized by radial filaments and clumps merging into a clumpy ring emitting in Hα, whereas an [O III] photograph shows that there is a swept-up shell which lies outside the Hα ring. Chu (1982) also studied the kinematics of RCW 58 with a Fabry–Perot Interferometer and found that the motion of the Hα ring is chaotic; unfortunately, no measurement of the expansion velocity of the swept-up shell is available because the [O III] line intensity was below her detection limit. Very recently, Kwitter (1984) has reported that RCW 58 appears to be enriched in helium and nitrogen by about a factor of 2.

In Section 2, we present high resolution *IUE* and optical spectra of the central WR star, HD 96548, which exhibit blueshifted absorption components in a number of interstellar lines arising from a variety of ions. In Section 3, we derive velocities and column densities for these components and show that their velocities are well correlated with the ionization potential of the corresponding ions, suggesting that the absorption originates behind a strong shock. In Sections 4 and 5 we discuss the likely origin of these components within a wind-blown bubble; we conclude that they probably arise behind the inwards-facing shock and show that our results require significant modifications to the standard wind-blown bubble model.

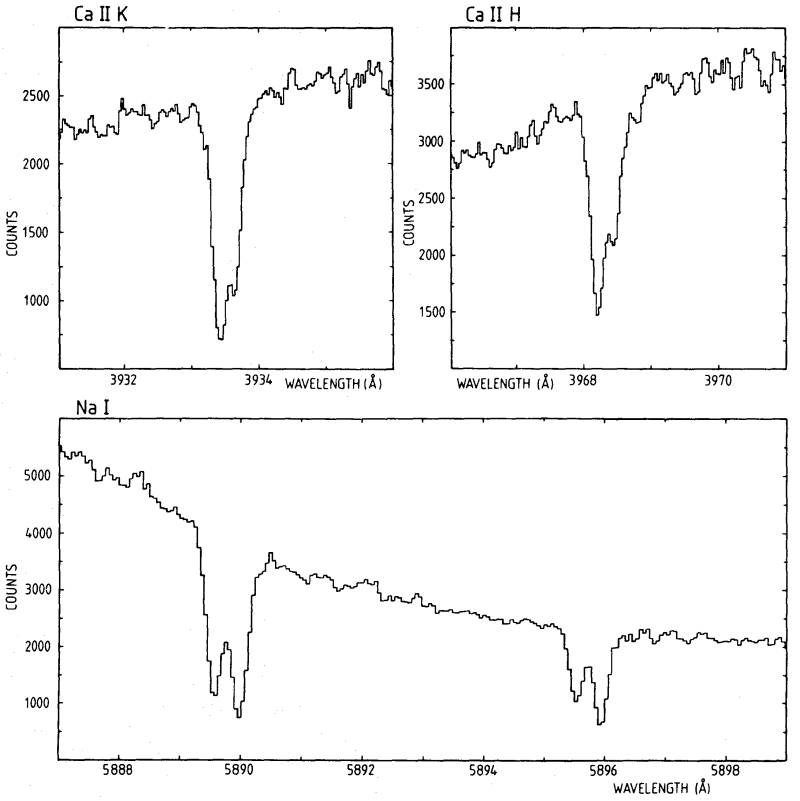

Figure 1. Portions of IPCS spectra of HD 96548, covering the Ca II and Na I interstellar lines, obtained with the AAT. The resolution is 10.8 km s^{-1} (Ca II) and 8.4 km s^{-1} (Na I); the signal-to-noise ratio is ~30–40.

2 Observations

2.1 OPTICAL OBSERVATIONS

We have obtained high resolution, high signal-to-noise ratio spectra of HD 96548 in the regions of the interstellar lines of Ca II $\lambda\lambda$ 3933, 3968 and Na I $\lambda\lambda$ 5889, 5895 as part of a survey of these lines in WR ring nebulae. The spectra were obtained in 1983 March at the Anglo-Australian Telescope (AAT), using the 82-cm camera of the RGO spectrograph with the IPCS; portions of the spectra including the interstellar Na I and Ca II lines are shown in Fig. 1. A 1200 lines mm^{-1} grating blazed at 12000 Å was used in second order to give a dispersion of 4.0 Å mm^{-1} at Na I, and in third order to give 2.7 Å mm^{-1} at Ca II. With this set-up and an IPCS format of 20×2048 channels, one 15 μm IPCS pixel covered 3.1 km s^{-1} at both Na I and Ca II; the resolution achieved was 8.4 and 10.8 km s^{-1} respectively, as indicated by the FWHM of comparison emission lines extracted and reduced in the same way as the data. Each spectrum was obtained by summing four consecutive 500 s exposures in which the stellar spectrum was typically spread over 2–3 of the 20 IPCS cross-sections, the remaining cross-sections being used to monitor the sky background. The star was moved on the slit between successive integrations so as to smooth the fixed-pattern noise by using different areas of the detector to record the spectrum. The effects of detector granularity were further reduced by dividing each 2-D data frame by a flat-field frame taken each night. Wavelength calibration was achieved by comparison with emission-line spectra of a Cu–Ar hollow-cathode lamp, taken at frequent intervals during each stellar exposure.

In the regions of interest, the reduced spectra have typically between ~2000 and ~4500 counts per wavelength bin above approximately 65 counts in the sky background; the corresponding signal-to-noise ratio of the data, as indicated by the rms deviation from the continuum level, is ~30–40.

Table 1. *IUE* high resolution observations of HD 96548.

Image No	Aperture Large/Small	Exposure Time (s)
SWP 4069	L	2700
SWP 6927	S	1800
SWP 7720	L	1500
SWP 10089	L	2880
SWP 10099	L	2700
SWP 13960	L	2400
SWP 13963	L	2400
SWP 13967	L	1439
SWP 13970	L	2400
SWP 16086	L	2700
LWR 3606	L	1200
LWR 6707	L	1500
LWR 10576	L	2220

2.2 IUE OBSERVATIONS

The WN8 star HD 96548 has been observed at high resolution ($\Delta\lambda \sim 0.1$–0.2 Å) with *IUE* by many investigators over the last five years. We have obtained from the World Data Centre all the available data [10 SWP (1150–2000 Å) and 3 LWR (1950–3300 Å) images]; details of these observations are given in Table 1. The spectra were reduced from their (G)PHOT images using the IUEDR software (Giddings 1983) available on the SERC STARLINK network of computers. This package has a number of significant advantages over the standard IUESIPS software aimed at maximizing the signal-to-noise ratio and resolution of the data. A better background subtraction is achieved by tracking each order individually and varying the height of the 'pseudo-slit' with order number. An empirical ripple correction, based on astronomical continuum spectra, is employed and any further fine adjustments such as improving the order overlaps or applying a background correction can be carried out interactively. We found this last facility essential for determining the zero level shortward of 1400 Å where the orders crowd together and consequently the background is poorly measured. In such cases we estimated the true background by reference to the cores of saturated interstellar lines. Any small wavelength shifts between different *IUE* images were accounted for by aligning the interstellar lines so that they matched those in SWP 13960. The *IUE* spectra were then summed to produce high signal-to-noise ratio absorption line profiles to enable us to detect reliably any weak interstellar components whose presence is uncertain in the single spectra. We checked that the resolution of the summed spectrum was not degraded by comparing the widths of selected interstellar lines with the corresponding values measured from the best exposed single spectrum. Examples of the major ultraviolet interstellar features in the summed spectrum are shown in Fig. 2.

3 Interstellar line components

3.1 VELOCITIES AND EQUIVALENT WIDTHS

In Table 2 we list equivalent widths and velocities (referred to the Local Standard of Rest) of individual resolved components of the optical and ultraviolet absorption lines. The error quoted for each equivalent width measurement is the 2σ error derived from the rms deviation of the fit to the local stellar continuum. We also give 3σ upper limits to the equivalent widths of absorption features of interest. As can be seen from Table 2, our detection limit for weak components is

Table 2. Equivalent widths and velocities of interstellar line components.

ION	I.P. (ev)	λ* (Å)	ABSORPTION LINE COMPONENTS					
			W_λ (mÅ)	v_{LSR} (km s^{-1})	W_λ (mÅ)	v_{LSR} (km s^{-1})	W_λ (mÅ)	v_{LSR} (km s^{-1})
NaI	5.139	5889.950	290 ± 20	-3	235 ± 20	-24	⩽ 18	
		5895.924	200 ± 15	-3	145 ± 10	-24	⩽ 18	
CaII	11.871	3933.663	165 ± 15	-5	200 ± 20	-24	⩽ 12	
		3968.468	100 ± 10	-5	145 ± 10	-24	⩽ 13	
MgII	15.035	2796.352			640 ± 45	-23	75 ± 15	-106
		2803.530			700 ± 45	-22	45 ± 15	-107
FeII	16.16	2600.172			505 ± 40	-19	35 ± 15	-102
SiII	16.345	1260.421			485 ± 40	-21	70:	-110
CII	24.383	1334.532			380:	-18	46 ± 7	-114
		1335.703			230 ± 15	-24	30 ± 6	-112
AlIII	28.448	1854.716			180 ± 10	-24	27 ± 6	-112
		1862.790			110 ± 7	-29	23 ± 7	-116
SiIII	33.492	1206.510			325 ± 55	-30	190 ± 25	-120
SiIV	45.141	1393.755			125 ± 25	-23	60 ± 20	-129
		1402.770			80 ± 10	-22	20 ± 7	-123
CIV	64.492	1548.188			200 ± 35	-30	65 ± 25	-147
		1550.762			100 ± 10	-35	20 ± 10	-150
UPPER LIMITS								
SiI	8.151	1255.276					⩽ 12	
		1845.520					⩽ 6	
OI	13.618	1302.168					⩽ 33	
NI	14.534	1199.550					⩽ 33	
SiII	16.345	1264.737					⩽ 12	
AlII	18.826	1670.787					⩽ 18	
NV	97.89	1238.808					⩽ 50	

Notes

* Wavelengths are in air for optical lines and in vacuum for UV lines

between ~5 and 50 mÅ, reflecting the varying signal-to-noise ratio of the *IUE* data which depends both on wavelength and on whether or not the local stellar continuum includes emission lines.

As can be seen from Fig. 1, the Ca II and Na I interstellar lines are split into two components. The blueshifted component occurs at the same velocity, $v_{LSR} = -24$ km s^{-1}, in Ca II and Na I. The velocity of the longer-wavelength component, however, appears to be slightly different between these two ions ($v_{LSR} = -5$ and -3 km s^{-1} respectively), suggesting that this component consists of at least two clouds with different proportions of Ca II and Na I.

Interstellar line velocities cannot normally be determined accurately from *IUE* data, due to uncertainties in the zero point of the wavelength scale. In our case this difficulty can be overcome by assuming that the velocity distribution of neutral species which are minor ionization stages in H I regions is similar to that of Na I, and that the corresponding absorption lines are centred at $v_{LSR} = -14$ km s^{-1} (the two Na I components at $v_{LSR} = -24$ and -3 km s^{-1} respectively are blended at the 25–30 km s^{-1} resolution of *IUE*). The mean velocity of 16 lines of C I, Cl I and S I in the *IUE* SWP wavelength range was measured to be $v_{SWP} = +14 \pm 5$ km s^{-1}, yielding a correction of -28 km s^{-1} to convert the observed velocities to an LSR frame of reference. In the *IUE* long-wavelength range we detect mainly lines of singly-ionized species (Fe II, Mn II and Mg II); an LWR correction of $+67$ km s^{-1} was derived by assuming that the main component of these lines is centred at the same velocity as other singly-ionized species detected in the SWP range.

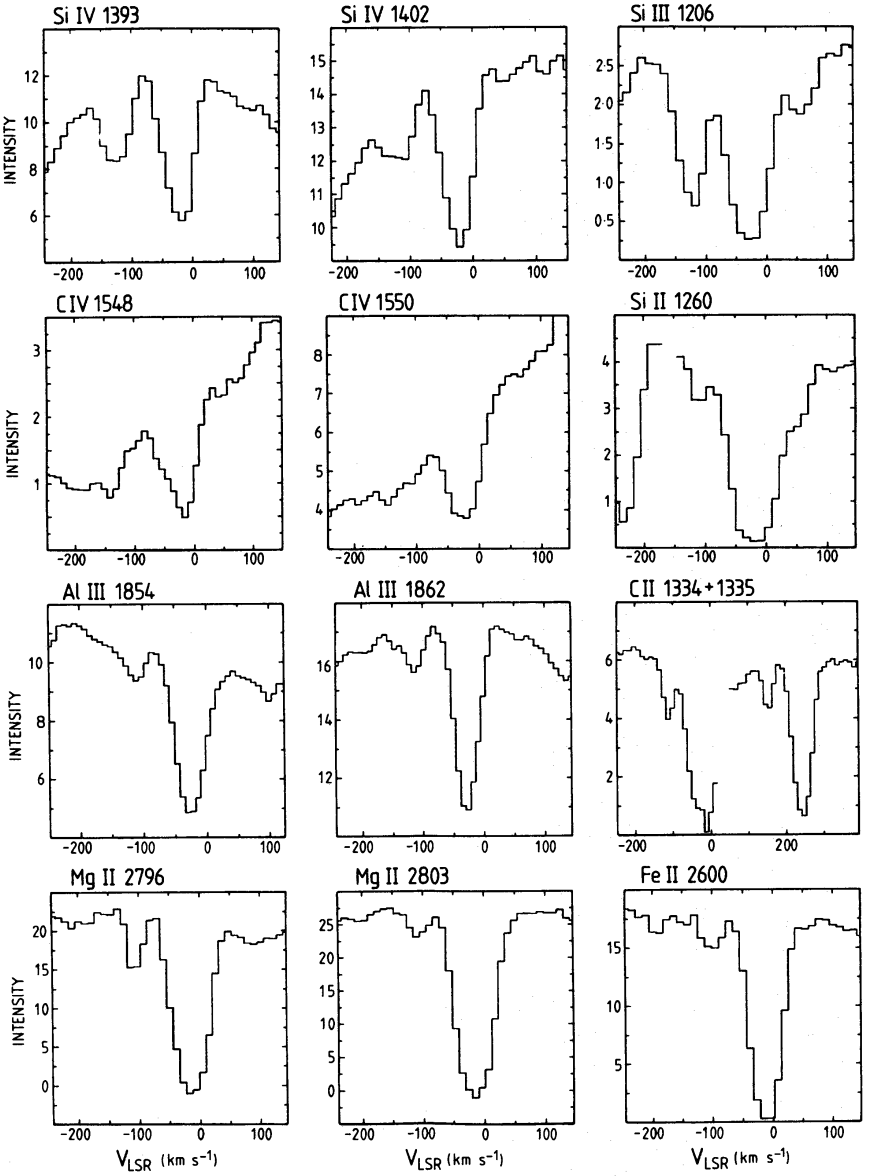

Figure 2. Examples of UV interstellar features observed in the summed *IUE* spectra of HD 96548. Each line profile is plotted on a velocity scale relative to the Local Standard of Rest.

As can be seen from Fig. 2, and from the equivalent width and velocity measurements collected in Table 2, the ultraviolet absorption lines show a main component centred at about $v_{LSR} = -24\,km\,s^{-1}$, and a weaker blueshifted component with velocity ranging from -102 to $-150\,km\,s^{-1}$. The former is a blend of the two components (at $v_{LSR} = -24$ and $\sim -4\,km\,s^{-1}$) resolved in Ca II and Na I and presumably includes additional absorption at higher negative velocities. The latter must be formed in a region where hydrogen is predominantly ionized, as indicated by the fact that it is strongest in Si III ($W_\lambda = 190$ mÅ), weak in lines of first ions and below the detection limit in all the neutral species within the *IUE* range, including O I and N I. This explains why this component is not seen, despite the very high signal-to-noise ratio of the data, in the optical lines which refer to minor ionization stages in H II regions.

Fig. 3 is a plot of the velocity of the blueshifted component seen in the ultraviolet lines as a function of ionization potential of the corresponding ion. It is immediately evident that there is a

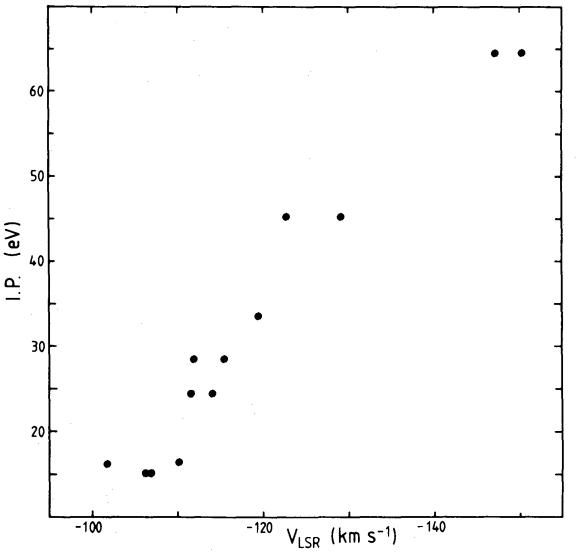

Figure 3. Velocities of the blueshifted components of the ultraviolet lines plotted as a function of ionization potential of the corresponding ions.

correlation between these two quantities, in the sense that ions with higher ionization potential appear at higher negative velocities. This correlation cannot be due to instrumental factors, since no similar effect is seen for the main, low-velocity component of the same absorption lines.

3.2 ION COLUMN DENSITIES

In order to deduce the column densities of the gas producing the different absorption components we have fitted theoretical profiles to the absorption lines, using the method described by Pettini *et al.* (1983). Initial estimates of the Doppler parameter, b, the central velocity, v_{LSR}, and the column density, N, for each component were used to generate a theoretical absorption line profile; the computed profile was then compared with the observed data points after convolution with the instrumental broadening function. [For the AAT data this was measured from the profiles of comparison Cu–Ar lamp lines extracted from the 2-D IPCS frames in the same way as the stellar data; for the *IUE* data we adopted the results of analogous measurements given by Boggess *et al.* (1978)]. The parameters of the model fit were subsequently adjusted until, by iteration, a satisfactory fit to the observations was achieved. We restricted the number of individual components used to fit each absorption line to be no greater than the number of components at least partially resolved; the value of the dispersion parameter b was constrained to be the largest compatible with the observed line profile. Examples of these models fits are shown in Fig. 4; absorption line parameters of individual components of interest are collected in Table 3.

A well known problem affecting the analysis of interstellar absorption lines is that the column densities derived in this way are strictly lower limits, in the sense that substantial column densities of gas in clouds of low-velocity dispersion can be masked by broader absorption (Nachmann & Hobbs 1973). This problem is particularly acute for the main component (at $v_{LSR} \approx -24$ km s^{-1}) of the ultraviolet lines, which undoubtedly is a blend of many distinct absorbing regions as indicated by its large width ($b \approx 30$ km s^{-1}). For this reason the column densities derived for this component are of little use and are not considered further here. Conversely, the high negative velocity component of the ultraviolet lines is generally weak (see Fig. 2), so that the corresponding column densities listed in Table 3 are unlikely to be in error by large factors. One possible exception is

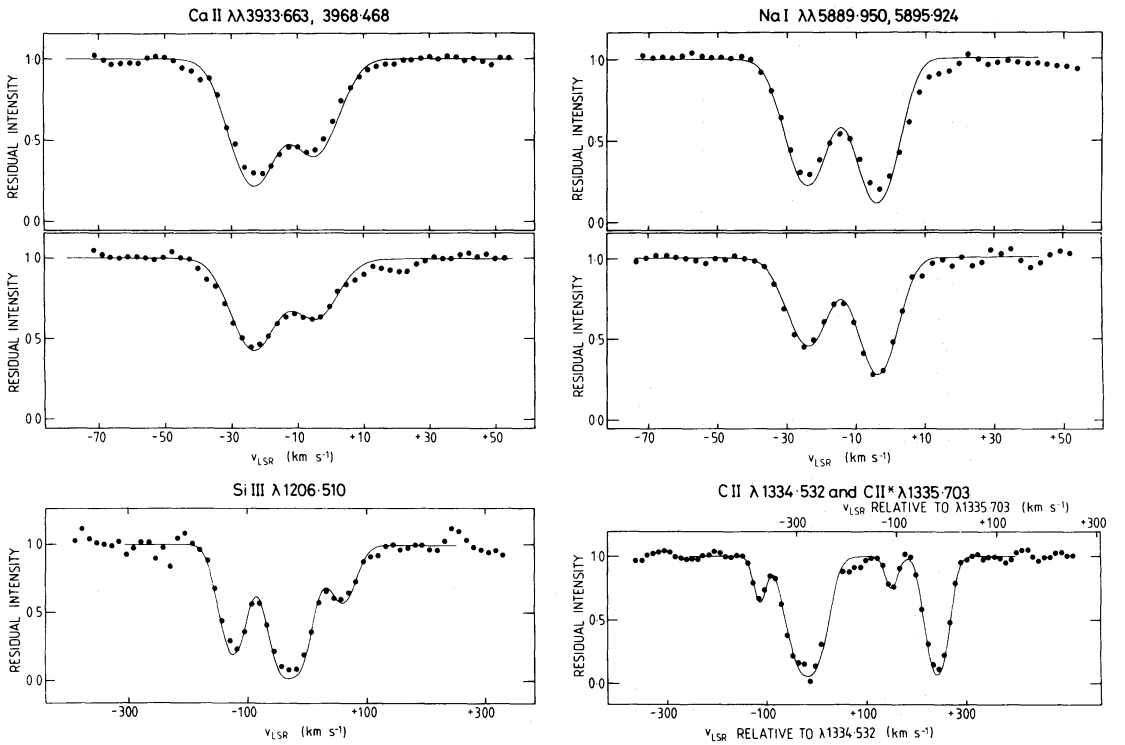

Figure 4. Velocity profiles of sample interstellar lines from the optical and ultraviolet spectra. The filled circles give the observed intensity normalized to the local stellar continuum. The continuous line shows the corresponding theoretical line profiles, convolved with the instrumental function and fitted to the data in order to derive estimates of the ion column densities.

Si III λ 1206.510, since the component is saturated in this line (see Fig. 4); consequently the column density of Si^{2+} may have been underestimated.

Turning to the optical lines, the component at $v_{LSR}=-24\,km\,s^{-1}$ is likely to be formed in a single 'cloud', as suggested by the good agreement, both in velocity and velocity dispersion, between the Na I and Ca II lines (see Table 3) and by the fact that a single component reproduces satisfactorily the profiles of the doublet lines (see Fig. 4). On the same grounds, the results of profile fitting indicate that the component at $v_{LSR}\approx-4\,km\,s^{-1}$ is probably an unresolved blend of at least two absorbing regions with differing proportions of Ca^+ and Na^0.

3.3 PROPERTIES OF THE COMPONENTS

In this section we apply the results of profile fitting to deduce relevant physical parameters of the resolved high-velocity components and suggest possible sites for the gas producing the absorption.

The component at $-24\,km\,s^{-1}$ resolved in Ca II and Na I occurs at a velocity greater than that expected for interstellar clouds in the line-of-sight to the star assuming that they participate in the galactic rotation. Although the distance of HD 96548 is not known accurately [recent estimates range from 4 kpc (Moffat & Seggewiss 1979) to 2 kpc (Conti *et al.* 1983)], this hardly affects the velocity expected from galactic rotation since $v_{LSR}=-14\,km\,s^{-1}$ for $d=2$ kpc and $-16\,km\,s^{-1}$ for $d=4$ kpc. Thus, this component may arise in an interstellar high-velocity cloud; such objects are commonly detected in high-resolution studies of the Na I and Ca II lines and usually exhibit a large Ca^+/Na^0 ratio (Siluk & Silk 1974), as indeed is the case here (see Fig. 4). An alternative possibility is that it may be associated with the clumps present in RCW 58. The Hα emission-line

Table 3. Parameters of profile fits.

Ion	b (km s^{-1})	v_{LSR} (km s^{-1})	N (10^{12}cm^{-2})
OPTICAL LINES			
Na^o	5.8	- 24	2.25
	5.0	- 3.5	3.7
Ca^+	5.8	- 24	4.1
	6.5	- 5	2.2
ULTRAVIOLET LINES			
C^+	10	-112	36 ± 6
C^{+*}	10	-112	23 ± 5
C^{3+}	11-13	-150	20 ± 10
N^o			$\leqslant$ 20
N^{4+}			$\leqslant$ 25
O^o			$\leqslant$ 50
Mg^+	10	-106	2.5 ± 0.5
Al^+			$\leqslant$ 0.5
Al^{2+}	10-15	-113	2.3 ± 0.6
Si^o			$\leqslant$ 1.5
Si^+	15:	-111	5.5:
Si^{2+}	24	-124	16.5 ± 4
Si^{3+}	20	-125	8 ± 2
Fe^+	15	-102	2.5 ± 1

profiles obtained by Chu (1982) for several regions of the nebula show more than 60 km s^{-1} of line broadening and splitting and extend up to velocities of -100 km s^{-1}. In this context, it is interesting to note that the major ultraviolet component is centred at -24 km s^{-1} and shows absorption extending up to $v_{LSR}=-50$ to -70 km s^{-1}; the strongest ultraviolet lines show an additional component at $+58$ km s^{-1} (e.g. Si III λ 1206.510, see Fig. 4). Although the velocities of these components are broadly consistent with the available emission-line data, accurate Hα profiles at the position of the star will be required to verify the suggested association of the gas seen in absorption with the Hα clumps.

As pointed out above, the velocity of the blueshifted ultraviolet component is well correlated with ionization potential in the sense that C IV has the highest negative velocity and Fe II the lowest (see Fig. 3). To our knowledge this is the first time that such a correlation has been observed. For this reason we consider it unlikely that this component arises in an intervening interstellar cloud, unrelated to RCW 58. More plausibly, we argue that we have detected shocked gas associated with the wind-blown bubble surrounding HD 96548. Before discussing the implications of the correlation shown in Fig. 3, we consider briefly the principal characteristics of the gas which can be deduced from the results of the absorption-line analysis. These are summarized in Table 4.

First, we note that the high-velocity component is of moderately high ionization, in the sense that the most populated ion stages of the elements observed appear to be one level above the dominant H I region species. The best tracer of the local ionization conditions is silicon, since lines from four successive ions are accessible with *IUE*. From Table 3 it can be seen that $Si^+:Si^{2+}:Si^{3+}=1:3:1.5$, while Si^0 is below our detection limit implying that $Si^+:Si^0>4$. Similarly, $Al^+:Al^{2+}<1:5$ and $C^+:C^{3+}=1:0.35$.

Secondly, we can capitalize on our good coverage of successive ionization levels of silicon to derive an estimate of the total column of gas moving at high negative velocities, assuming a solar abundance ($Si/H_\odot=3.5\times10^{-5}$, Snow 1980). From the silicon column densities in Table 3, $N(H)\gtrsim1\times10^{18}$ cm^{-2}; this is a lower limit primarily because: (1) we may have underestimated the column density of Si^{2+}, as explained above, and (2) we do not observe Si^{4+}. We can further use this estimate of the total column density to deduce lower limits to the ionization fraction of

Table 4. Summary of physical parameters of shocked gas.

Total hydrogen column density	$N(H) \geqslant 1 \times 10^{18}$ cm^{-2}
Ionisation fraction	$= N(H^+)/N(H^0) > 10$
Electron density	$< n_e T_4^{-0.5} >_{CII} \simeq 25$cm^{-3}
Hydrogen recombination time	$< t_r T_4^{-0.16} >_{CII} \simeq 3 \times 10^3$ years
Abundances (C, Mg, Al, Si, Fe)	≈ Solar

hydrogen in the high-velocity gas from the absence of O I and N I absorption. These limits are based on the assumptions that the abundance of O and N are at least solar (which is likely, as discussed below) and that the ionization fractions of H, O and N are comparable, since these elements have very similar ionization potentials (13.598, 13.618 and 14.534 eV respectively) and are closely coupled by charge transfer reactions (Field & Steigman 1971; Chambaud *et al.* 1980). The upper limit $N(0^0)<5\times10^{13}\,\mathrm{cm}^{-2}$ in Table 3 then implies $f=N(H^+)/N(H^0)>10$ ($O/H_\odot=6.75\times10^{-4}$, Snow 1980); a less stringent limit $f>4$ is obtained from the observed $N(N^0)<2\times10^{13}\,\mathrm{cm}^{-2}$ and $N/H_\odot=1.15\times10^{-4}$.

Thirdly, we point out that the relative column densities of the first ions are close to the elements' solar abundances. From Table 3 it can be seen that $Si^+:C^+:Mg^+:Fe^+:Al^+=1:11:0.5:0.5:<0.1$, to be compared with the corresponding solar ratios: 1:10.5:1:0.7:0.07 (Snow 1980). If the ionization corrections for unobserved ion stages do not differ by large factors among the above elements, this would suggest that the chemical composition of the high-velocity gas is approximately solar, since in low-velocity interstellar clouds these elements are normally depleted by largely differing amounts (e.g. Morton 1975; Hobbs, York & Oegerle 1982). This result is in line with expectations that interstellar grains are destroyed in high-speed shocks (Seab & Shull 1983) as confirmed by observations of supernova remnants (e.g. Jenkins, Silk & Wallerstein 1976; Phillips & Gondhalekar 1983; Paul *et al.* 1985). The recently discovered over-abundances of He and N (Kwitter 1984) indicate that RCW 58 consists, at least in part, of processed WN stellar wind material. These over-abundances, however, are not inconsistent with our finding that the high-velocity gas responsible for the ultraviolet absorptions has an approximately solar composition, since He and N are the only elements expected to be enriched in the stellar wind of HD 96548 (Smith & Willis 1983). Unfortunately, we are unable to confirm independently the over-abundance of N with the present analysis; the expected dominant ions N^+ and N^{2+} have resonance transitions below the *IUE* wavelength range and the lower limits we are able to place on the column densities of N^0 and N^{4+} are not very instructive in this context.

From Fig. 4 it can be seen that we detect high negative velocity components in both the fine-structure and ground state transitions of C^+. The degree of excitation of the fine-structure levels of C^+ can be used to derive further information on the physical conditions. The high fractional ionization deduced for the gas implies that collisions with electrons are likely to be the major mechanism populating the excited level with $J=3/2$; the fractional column density in the latter relative to the ground state with $J=1/2$ then gives a measure of the quantity $\langle n_e\, T_4^{-0.5}\rangle$ (T_4 being the temperature in units of 10^4 K), which is a line-of-sight average weighted by the local ion density (Bahcall & Wolf 1968). The observed ratio $N(C^{+*})/N(C^+)=0.65\pm0.2$ (Table 3) implies $\langle n_e\, T_4^{-0.5}\rangle_{C\,II}\simeq25\,\mathrm{cm}^{-3}$; the lack of detectable fine-structure excitation of Si^+ is consistent with this value ($\langle n_e\, T_4^{-0.5}\rangle_{Si\,II}<150\,\mathrm{cm}^{-3}$). Using the approximation given by Jenkins *et al.* (1976), the above electron density corresponds to a hydrogen recombination time $\langle t_r\, T_4^{-0.16}\rangle_{C\,II}\simeq3\times10^3$ yr, which is only weakly dependent on the temperature of the gas. It must be emphasized that these estimates of electron density and hydrogen recombination time only apply to the region of shocked gas which has already cooled to temperatures appropriate to C^+.

4 Kinematic considerations

For the purposes of this paper we confine ourselves to a semi-qualitative discussion. More detailed quantitative calculations will be presented in a subsequent paper (Dyson, Hartquist, Pettini & Smith (in preparation – henceforth DHPS). Fig. 3 shows that the velocity of each blueshifted ultraviolet component is linearly proportional to its ionization potential in the sense that C IV has the highest negative velocity and Fe II the lowest. The sense of this correlation immediately rules out the possibility that the absorption lines originate in the swept-up shell of interstellar material surrounding HD 96548. The swept-up shell is bounded by an outwards-facing shock which is moving towards the observer. Low-velocity interstellar gas passing through this shock is initially heated and, as it cools in the subsonic flow, its velocity approaches that of the shock itself. Hence, in the observer's frame of reference, the gas becomes progressively more blueshifted as it cools leading to a relationship between ionization potential and velocity opposite to that observed in Fig. 3. The 'standard' model of a stellar wind interacting with the interstellar medium (*cf.* Dyson 1981) also possesses an inwards-facing shock located between the stellar wind and the hot bubble. Stellar wind material entering this shock is decelerated as it cools and thus becomes progressively *less* blueshifted in the observer's frame of reference. Therefore we will argue that the detected absorption features arise in a region between the inwards-facing shock and the shell of ambient material swept up by the outwards-facing shock. However, very significant modifications to the standard model are required by the observations. We will employ the phrase 'simple flow' to refer to the situation where the gas flows both upstream and downstream of an inwards-facing shock contain no irregularities. The term 'non-simple flow' will be used for flows containing irregularities. We now show that for observational and theoretical reasons a simple flow cannot be used to explain the results.

By far the most striking feature of the observations is the linear correlation between the ionization potential of a species and the radial velocity at which it is observed. This correlation would be anticipated if three conditions were satisfied in the absorbing region, namely: (1) collisional ionization equilibrium with the ionization potential IP of the observed species directly proportional to the temperature T of the gas in which it exists, IP $\propto T$; (2) isobaric subsonic flow, $P \propto \varrho T = \text{const.}$, where ϱ is the gas density; and (3) steady flow in a thin region with mass conservation $\varrho v = \text{const.}$, where v is the flow velocity. (The relationship IP $\propto v$ clearly follows.)

Leaving aside for the moment the implications of ionization equilibrium, we can easily demonstrate that it is not possible to reproduce the measured slope of the IP–velocity (or equivalently, temperature–velocity) diagram by a simple flow. Under the assumptions listed above, the gas pressure P is given by $P \cong (\mathscr{R}/\mu)\varrho T$, where $\mu (\approx 1/2)$ is the gas molecular weight and $\mathscr{R}$ the gas constant. Mass conservation is $\varrho v = \varrho_1 v_1$ where v is the flow speed relative to the shock and the subscript denotes conditions in the immediate pre-shock gas. From the strong jump conditions, $P = 3\varrho_1 v_1^2/4$, hence $v = 4\mathscr{R}T/(3\mu v_1) \cong 2.2\times 10^8\, T/v_1\ \mathrm{cm^{-1}}$. The observed velocity difference between the regions where the C^{3+} features and the features produced by more lowly ionized species originate is about $45\ \mathrm{km\,s^{-1}}$ (Fig. 3). If there is ionization equilibrium, the temperature difference between these regions is about 10^5 K. Hence $v_1 \approx 50\ \mathrm{km\,s^{-1}}$. But the temperature produced behind a shock with this upstream flow velocity is $T_s \approx 3.5\times 10^4$ K, far too low to produce a substantial amount of C^{3+}. In fact, for values of v_1 sufficiently high to produce C^{3+} ($v_1 > 85\ \mathrm{km\,s^{-1}}$), the simple flow model predicts a velocity spread of less than $25\ \mathrm{km\,s^{-1}}$; this value is excluded by the observations presented in Fig. 3. Thus the slope of the observed T–v correlation is too small implying that the assumption of a simple flow behind an inwards-facing shock cannot be correct. An important way of interpreting this discrepancy is that the ratio $\varrho v/P$ is too small behind such a shock (since the slope is $2.2\times 10^8/v_1$ and $v_1 = 4P/3\varrho v$). Flow modifications which enhance this ratio in the post-shock gas are an obvious circumvention of this problem.

As discussed above, in order to explain the relationship IP$\propto v$ in the post-shock flow, we require that IP$\propto T$. This is a reasonable description of the ionization distribution of plasma in collisional ionization equilibrium. The fact that equilibrium conditions are required to reproduce the observed ionization potential–velocity proportionality has important implications. At a temperature of about 10^5 K, the approximate recombination time for C^{3+} is $t_R \approx 10^{12}/n_e$ s, where n_e is the local electron density (Aldrovandi & Péquignot 1973). The cooling time is $t_c \approx 5\times10^{10}/n_e$ s (Summers & McWhirter 1979). Since $t_c < t_R$, collisional ionization equilibrium cannot be maintained unless there is some means of injecting energy into the gas to increase the effective cooling time. A possible heating source is the decay of subsonic turbulence. [The velocity dispersions derived for the blueshifted components of the absorption lines (see Table 3) are consistent with the presence of internal turbulence.]

Suppose that the turbulent energy density, E_t, is a factor $f(\lesssim 1)$ times the thermal energy density, E_{th}, and that the turbulence decays on a characteristic time-scale $t_d \approx \lambda/v_T$. (Here λ is the characteristic eddy size and v_T is the turbulent velocity). For any significant effect, $(E_t/t_d) \approx (E_{th}/t_c)$, i.e. $\lambda \approx 10^{17} f\,(v_T/20\,\mathrm{km\,s^{-1}})\,n_e^{-1}$ cm. The estimated lower limit to the column density of this region derived in Section 3.3 is $N_H \gtrsim 10^{18}\,\mathrm{cm^{-2}}$. Thus $(\lambda/L) \lesssim 0.1\,f\,(v_T/20\,\mathrm{km\,s^{-1}})$, where L is the scale size of the absorbing region. This is not an implausible requirement but does suggest that the turbulence is on a macroscopic scale.

An additional constraint must be put on the flow, namely that the flow time across this region must be at least comparable with the recombination time t_R. The flow time is $t_f \approx L/v \approx 2\times10^{11}$ $(N_H/10^{18}\,\mathrm{cm^{-2}})$ $(v/45\,\mathrm{km\,s^{-1}})\,n_e^{-1}$ s. Thus for $t_R \lesssim t_f$, $N_H \gtrsim 5\times10^{18}\,\mathrm{cm^{-2}}$, which is not inconsistent with the lower limit of $1\times10^{18}\,\mathrm{cm^{-2}}$ implied by the observed Si column density assuming solar abundances.

There are further strong arguments in favour of abandoning the standard wind-interaction model. In these models, the immediate post-shock wind gas has a temperature $T_s \gtrsim 10^7$ K with the wind speeds ($\gtrsim 10^3\,\mathrm{km\,s^{-1}}$) characteristic of WR stars. The expansion lifetime of a simple wind-blown bubble of radius R and expansion speed V_e is $t_L \approx (3/5)\times R/V_e \approx 3\times10^4$ $(R/5\,\mathrm{pc})$ $(V_e/100\,\mathrm{km\,s^{-1}})^{-1}$ yr. This is far less than the time-scale for radiative cooling in the shocked-wind gas. There are two other ways of producing cooled gas. Shocked-wind gas near the contact discontinuity separating shocked stellar wind and shocked ambient gas has an increasing density and decreasing temperature towards the contact discontinuity (Falle 1975). The velocity of this gas with respect to the star decreases outwards. Thus the theoretical T–v correlation is as observed. However it can readily be shown (DHPS) that the observed slope of the T–v correlation cannot be fitted by this model under any circumstances. In a modification of the standard model, Weaver *et al.* (1977) suggest that the hot shocked stellar wind produces evaporation of cool swept-up material at the interface. However, in the reference frame of the star, the hottest gas has the lowest outwards velocity which is directly opposite to the sense of the observations (Fig. 5 is a sketch of the velocity and temperature distributions across the conduction front).

We must clearly abandon the standard model. The necessity to raise the ratio $\rho v/P$ behind an inwards-facing shock and the discussion on ionization equilibrium above leads us to propose a non-simple flow in which hot shocked stellar wind material mixes with cold material and cools as it flows outwards and decelerates. Fig. 6 shows a schematic representation of the structure envisaged to produce a non-simple flow. Here the cold material is represented by dense blobs of gas occurring throughout the bubble. The clumps located near the inwards-facing shock are progressively eaten away by the initially very hot ($T \sim 10^7$ K) shocked stellar wind. The shocked material then gradually cools through mixing as it flows outwards and decelerates. The ultraviolet absorption features are formed in this cooler shocked gas which is naturally turbulent because of the complicated flow pattern. However, one feature of the standard model which we retain is that

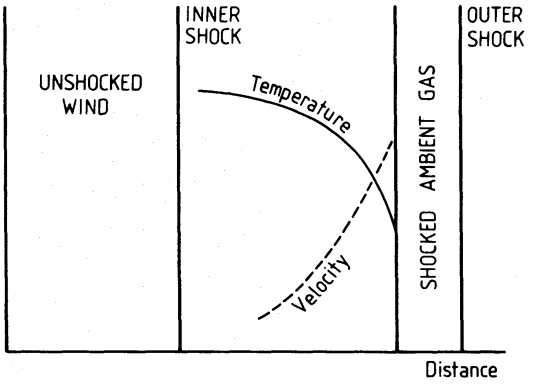

Figure 5. Sketch of the velocity (relative to the stellar reference frame) and temperature structure across a conduction front as in the model of Weaver *et al.* (1977). The hottest gas has the lowest outward velocity which is directly opposite to the sense of the observations reported here.

this region as a whole must move outwards with a velocity of about 100 km s^{-1} with respect to the star in order to explain the x-axis intercept of the ionization potential/velocity relation (Fig. 3). Clearly, Fabry–Perot observations of the [O III] shell are of crucial importance since a measurement of the expansion velocity will directly test the proposed model.

5 Energy considerations

In Section 1, Chu's (1982) comparison of Wolf–Rayet nebula energetics with the predictions of the standard wind interaction model was discussed and the existence of large kinetic energy deficiencies in the expanding nebulae was noted. There are at least two possible explanations for

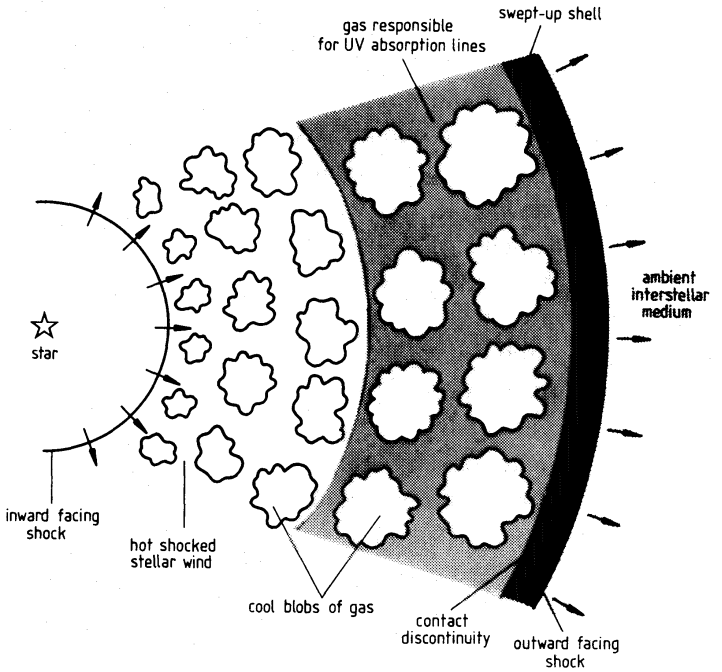

Figure 6. Schematic representation (not drawn to scale) of the structure of RCW 58 proposed to explain the observed linear correlation between the ionization potential of an ionized species and the velocity at which the absorption line is formed. As discussed in the text, this model can account for the fact that the kinetic energy required to drive the shell expansion is only a small fraction of that provided by the stellar wind, contrary to expectations for a simple flow.

this. The dynamical ages of the nebulae (which are assumed also to be the time-scales for the fast WR wind energy injection) are obtained from the observed nebular radii and expansion velocities. However, if a nebula originates from an interaction between a stellar wind and a previously generated shell of material (the radius of which is about equal to the observed nebular radius), the actual duration of wind activity is the nebular radius divided by the wind speed, considerably less than the previous estimates. Possible mechanisms for producing this type of interaction include the wind activity of an O star progenitor, a supernova event or impulsive ejection in a red supergiant phase. The WR ring nebula NGC 6888 may be an example of this mechanism since the observed He and N enrichment and the low mass ($\sim 3.6\,M_\odot$; Kwitter 1981) suggest that the nebula may be composed primarily of stellar ejecta. Alternatively, the observed overabundances in NGC 6888 may be caused by continuous stellar wind enrichment, although it is difficult to understand how this material can cross the contact discontinuity between the bubble and shell.

Another possibility is that the simple dynamical age estimates of WR ring nebulae are correct, but then some means of increasing the radiative losses from the shocked wind must be found. The mixing of cool ambient material into the shocked-wind gas may achieve this result. Chu (1982) estimates a mass M_s of about $3\,M_\odot$ for RCW 58. The measured mean radius of about 3.5 pc (Chu 1982) and the expansion velocity V_e of $100\,\mathrm{km\,s^{-1}}$ postulated previously give a dynamical age $t \simeq 2\times10^4$ yr. The resulting energy conservation parameter $\varepsilon = M_s V_e^2 / \dot{M}_w V_w^2\, t$ is $\sim 1.5\times10^{-2}$ assuming that the mass loss rate $\dot{M}_w$ of HD 96548 is $3\times10^{-5}\,M_\odot$/yr (Barlow, Smith & Willis 1981) and the wind terminal velocity V_w is $1800\,\mathrm{km\,s^{-1}}$ (Willis 1982). The derived value for ε is about a factor of 15 lower than that predicted by the standard model; this suggests that one or other of the above mechanisms is operative here. We propose that this global energy discrepancy is related to the model we have put forward to explain the observed velocity/ionization potential correlation. If mixing does occur behind the wind shock (at roughly the post-shock pressure), then the mass injection will increase the ratio $\rho v/P$ as required by the discussion above. The mixing process will, moreover, lower the temperature of the shocked stellar wind which will then lose energy efficiently by radiative cooling. The enhanced helium and nitrogen abundances (Kwitter 1984) together with the morphology of RCW 58 do indeed indicate that the nebula is composed of clumpy dense stellar ejecta which could be the source of the required mass. Detailed models (DHPS) will provide constraints on the parameters of the interaction.

If the above interpretation is correct, the large kinetic energy deficiencies observed in NGC 6888 and RCW 58 could be the result of two different mechanisms, although both require that the nebulae are composed mainly of stellar ejecta. Their strong morphological dissimilarity supports this idea, since NGC 6888 appears to be a wind-driven shell of ejecta, whereas RCW 58 has clumps of stellar ejecta within its wind-blown bubble rather than a well defined shell.

Clearly it is important to search for high-velocity absorption components in other WR ring nebulae since further examples may improve our understanding of the formation and subsequent evolution of these nebulae. In particular, it is important to establish if the correlation discovered in RCW 58 between ionization potential and component velocity is a common feature of this class of objects as this would argue for a common origin. High negative velocity absorption has been reported in NGC 6888 (Huber *et al.* 1979); however, only high-ionization species were observed and recent work has shown that these components could be formed in a large-scale shell expanding away from the Cyg OB1 association (Phillips, Welsh & Pettini 1984). Blueshifted absorption features covering a wide ionization range have also been detected in the *IUE* spectra of HD 50896, a WN5 star surrounded by the wind-blown bubble S308, but their interpretation is still somewhat controversial (Shull 1977; Smith, Willis & Wilson 1980; Smith 1982; Howarth and Phillips 1984, in preparation). The detection of ultraviolet absorption lines associated with other WR ring nebulae is therefore yet to be confirmed.

References

Aldrovandi, S. M. V. & Péquignot, D., 1973. *Astr. Astrophys.*, **25,** 137.
Avedisova, S., 1972. *Soviet Astr.*, **15,** 708.
Bahcall, J. N. & Wolf, R. A., 1968. *Astrophys. J.*, **152,** 701.
Barlow, M. J., Smith, L. J. & Willis, A. J., 1981. *Mon. Not. R. astr. Soc.*, **196,** 101.
Boggess, A. *et al.* 1978. *Nature,* **275,** 377.
Chambaud, G., Launay, J. M., Levy, B., Millie, P., Roueff, E. & Tran Minh, F., 1980. *J. Phys. B: Atom. Molec. Phys.*, **13,** 4205.
Chu, Y. H., 1981. *Astrophys. J.*, **249,** 195.
Chu, Y. H., 1982. *Astrophys. J.*, **254,** 578.
Conti, P. S., Garmany, C. D., de Loore, C. & Vanbeveren, D., 1983. *Astrophys. J.*, **274,** 302.
Crampton, D., 1971. *Mon. Not. R. astr. Soc.*, **153,** 303.
Dyson, J. E., 1981. *Investigating the Universe,* p. 125, ed. F. D. Kahn, Reidel, Dordrecht, Holland.
Dyson, J. E. & de Vries, J., 1972. *Astr. Astrophys.*, **20,** 223.
Falle, S. A. E. G., 1975. *Astr. Astrophys.*, **43,** 323.
Field, G. B. & Steigman, G., 1971. *Astrophys. J.*, **166,** 59.
Giddings, J. R., 1983. *IUE ESA Newsletter No. 17,* 53.
Heckathorn, J. N., Bruhweiler, F. C. & Gull, T. R., 1982. *Astrophys. J.*, **252,** 230.
Hobbs, C. M., York, D. G. & Oegerle, W., 1982. *Astrophys. J.*, **252,** L21.
Huber, M. C. E., Nussbaumer, H., Smith, L. J., Willis, A. J. & Wilson, R., 1979. *Nature,* **278,** 697.
Jenkins, E. B., Silk, J. & Wallerstein, G., 1976. *Astrophys. J. Suppl.*, **32,** 681.
Johnson, H. M. & Hogg, D. E., 1965. *Astrophys. J.*, **142,** 1033.
Kwitter, K. B., 1981. *Astrophys. J.*, **245,** 154.
Kwitter, K. B., 1984. *Astrophys. J.*, in press.
Moffat, A. F. J. & Seggewiss, W., 1979. *Astr. Astrophys.*, **77,** 128.
Morton, D. C., 1975. *Astrophys. J.*, **197,** 85.
Nachmann, P. & Hobbs, L. M., 1973. *Astrophys. J.*, **182,** 481.
Paul, J. A., Laurent, C., Pettini, M., Vidal-Madjar, A. & Oliver, M. B., 1985. *Astrophys. J.*, in press.
Pettini, M., Hunstead, R. W., Murdoch, H. S. & Blades, J. C., 1983. *Astrophys. J.*, **273,** 436.
Phillips, A. P. & Gondhalekar, P. M., 1983. *Mon. Not. R. astr. Soc.*, **202,** 483.
Phillips, A. P., Welsh, B. Y. & Pettini, M., 1984. *Mon. Not. R. astr. Soc.*, **206,** 55.
Pikel'ner, S. B., 1968. *Astrophys. Lett.*, **2,** L97.
Seab, C. G. & Shull, J. M., 1983. *Astrophys. J.*, **275,** 652.
Shull, J. M., 1977. *Astrophys. J.*, **212,** 102.
Siluk, R. S. & Silk, J., 1974. *Astrophys. J.*, **192,** 51.
Smith, L. J., 1982. *PhD. thesis,* University of London.
Smith, L. J. & Willis, A. J., 1983. *Mon. Not. R. astr. Soc.*, **201,** 451.
Smith, L. J., Willis, A. J. & Wilson, R., 1980. *Mon. Not. R. astr. Soc.*, **191,** 339.
Snow, T. P., 1980. *ESA Workshop on the Interstellar Medium,* Villafranca del Castillo, unpublished.
Summers, H. P. & McWhirter, R. W. P., 1979. *J. Phys. B: Atom. Molec. Phys.*, **12,** 2387.
Treffers, R. R. & Chu, Y. H., 1982. *Astrophys. J.*, **254,** 569.
Weaver, R., McCray, R., Castor, J. I., Shapiro, P. R. & Moore, R., 1977. *Astrophys. J.*, **218,** 377.
Wendker, H. J., Smith, L. F., Israel, F. P., Habing, H. J. & Dickel, H. R., 1975. *Astr. Astrophys.*, **42,** 173.
Willis, A. J., 1982. *Mon. Not. R. astr. Soc.*, **198,** 897.